Fraunhofer computer-generated hologram for diffused 3D scene in Fresnel region

Yuan-Zhi Liu,[1] Jian-Wen Dong,[1,3] Yi-Ying Pu,[1] He-Xiang He,[1] Bing-Chu Chen,[1] He-Zhou Wang,[1,4] Huadong Zheng,[2] and Yingjie Yu[2]

[1]State Key Laboratory of Optoelectronic Materials and Technologies, Sun Yat-sen (Zhongshan) University, 510275, Guangzhou, China

[2]Department of Precision Mechanical Engineering, Shanghai University, 200072, Shanghai, China

[3]e-mail: dongjwen@mail.sysu.edu.cn

[4]e-mail: stswhz@mail.sysu.edu.cn

Received February 7, 2011; revised April 14, 2011; accepted April 29, 2011; posted May 2, 2011 (Doc. ID 142296); published June 1, 2011

A Fraunhofer computer-generated hologram (CGH) is proved to be valid in display for three-dimensional (3D) objects from the Fresnel to the far-field region without a Fourier lens for reconstruction. To quickly compute large and complicated 3D objects that consist of slanted diffused surfaces in the Fresnel region, a Fraunhofer-based analytical approach using a basic-triangle tiling diffuser is developed. Both theoretical and experimental results reveal that Fraunhofer CGH can perform the same effects as Fresnel CGH but require less calculation time. Impressive 3D solid effects are achieved in the Fresnel region.

OCIS codes: 090.0090, 090.1760, 090.2870.

Three-dimensional display has attracted tremendous attention [1–17]. The computer-generated hologram (CGH) is a promising technique for 3D display [1–3]. For the flexibility of controlling all aspects of an optical wave, it can produce the most accurate depth cues for 3D objects that exist or never exist in the real world [1].

An important issue regarding CGHs is the computation of propagation. For convenient observation, objects in different depths are usually located within the Fresnel region. Fresnel diffraction is naturally used to calculate 3D imaging with considerable depth-of-field (DOF). But it is difficult to reduce computational complexity while maintaining a full parallax effect [3,7]. Recently, methods of wave propagation on either parallel planes [8,9] or slanted planes [10,11] were developed, which can be applied to calculate Fresnel diffraction. Some researchers proposed analytical Fourier spectrum methods to decrease the computational complexity [12,13].

Optical Fraunhofer holography is usually considered as a method that can only be applied in the far-field region. Distance between objects and the hologram need to be very large, or the size of objects need to be very small [3,14]. People take for granted that Fraunhofer CGH (Fh-CGH) has asimilar restriction. It is thought that the reconstruction performance of a Fh-CGH is similar to that of a Fourier CGH. So a Fourier lens is usually needed for optical recreation, and the DOF is shallow. Another important aspect of the Fh-CGH is how to employ a digital diffuser to uniformize the Fourier spectrum [2]. This is challenging for the case of slanted planes in an analytical Fourier spectrum method. Until recently, an inspiring approach was proposed using triangular subdivision [12].

In this Letter, we prove that Fh-CGH can image 3D objects from the Fresnel to the far-field region. We show that Fh-CGH performs the same effects as Fresnel CGH (Fr-CGH). A highly efficient approach based on basic-triangle tiling is analytically derived to encode Fh-CGH for 3D diffusive objects composed by slanted triangle meshes. Optical reconstructions reveal a high quality 3D solid effect.

Consider a planar object (at $z < 0$) with complex amplitude $\mathcal{O}_o$ parallel to the hologram ($z = 0$) within the Fresnel region. The object wave distribution across the hologram can be calculated by the Fresnel formula [1]:

$$\mathcal{O}_H^{\mathrm{Fr}}(x_H, y_H) = [\exp(j2\pi z/\lambda)/j\lambda z]\mathcal{Q}(x_H, y_H) \iint \mathcal{O}_o(x_o, y_o) \times \mathcal{P}(x_o, y_o) \exp[-j2\pi(x_H x_o + y_H y_o)/\lambda z]\mathrm{d}x_o\mathrm{d}y_o, \quad (1)$$

where $j = \sqrt{-1}$, $\mathcal{P} = \exp[j\pi({x_o}^2 + {y_o}^2)/\lambda z]$, $\mathcal{Q} = \exp[j\pi({x_H}^2 + {y_H}^2)/\lambda z]$. λ is the wavelength. (x_o, y_o) and (x_H, y_H) are the coordinate systems of the object and the hologram, respectively. If $\mathcal{P}$ is discarded, Eq. (1) becomes the Fraunhofer diffraction:

$$\mathcal{O}_H^{\mathrm{Fh}}(x_H, y_H) = [\exp(j2\pi z/\lambda)/j\lambda z]\mathcal{Q}(x_H, y_H)\mathcal{F}[\mathcal{O}_o(x_o, y_o)], \quad (2)$$

where $\mathcal{F}[\cdot]$ stands for the Fourier transform (FT) evaluated at frequencies $(x_H/\lambda z, y_H/\lambda z)$. A plane wave $R_H = R_0 \exp[j2\pi(x_H \cos\alpha + y_H \cos\beta)/\lambda]$, is used as reference light to encode the Fr-CGH and Fh-CGH by Eqs. (1) and (2), respectively. Here, (α, β) are angles with respect to the (x_H, y_H) axis. Fresnel diffraction is adopted to describe the optical reconstruction process with the same reference light for both CGHs. After simple derivations, we have the expressions of complex amplitude of virtual and real images at $-z$ and z, respectively, which are ${\mathcal{O}_{\mathrm{virt}}}^{\mathrm{Fr}} = \mathcal{O}_o(x', y')$ and ${\mathcal{O}_{\mathrm{real}}}^{\mathrm{Fr}} = \exp\{-j4\pi[(x'\cos\alpha - z\cos^2\alpha) + (y'\cos\beta - z\cos^2\beta)]/\lambda\}\mathcal{O}_o^*(x' - 2z\cos\alpha, y' - 2z\cos\beta)$ for Fr-CGH, while ${\mathcal{O}_{\mathrm{virt}}}^{\mathrm{Fh}} = \exp[-j\pi(x'^2 + y'^2)/\lambda z]\mathcal{O}_o(x', y')$ and ${\mathcal{O}_{\mathrm{real}}}^{\mathrm{Fh}} = \exp[j\pi(x'^2 + y'^2)/\lambda z]\mathcal{O}_o^*(x' - 2z\cos\alpha, y' - 2z\cos\beta)$ for Fh-CGH. Here, (x', y') is the coordinate system of the reconstruction plane. The complex amplitudes carrying the information of objects are the same in both CGHs results [e.g. $\mathcal{O}_o(x', y')$ for a virtual image and $\mathcal{O}_o^*(x' - 2z\cos\alpha, y' - 2z\cos\beta)$ for a real image]. The only

differences between $\mathcal{O}_{\text{virt}}^{\text{Fr}}(\mathcal{O}_{\text{real}}^{\text{Fr}})$ and $\mathcal{O}_{\text{virt}}^{\text{Fh}}(\mathcal{O}_{\text{real}}^{\text{Fh}})$ are additional phase factors. However, human eyes can just receive intensity of light. For the purpose of display, people are concerned only with intensity of reconstruction rather than its complex amplitude. Therefore, the display reconstruction performances of two such CGHs should be the same. To examine this statement, we encode a square aperture (with the width of $2w$) into holograms and reconstruct it numerically. Normalized error power [15] is used to compare the reproduced image's intensity with the original object. Note that the normalized error power here is the ratio of intensities while it is the ratio of complex fields in [15]. The Fresnel number is defined as $Nf = w^2/\lambda z$. When $Nf \ll 1$, the object is in the far-field region; while $Nf \geq 1$, it is deemed to be in the Fresnel region [1,3]. Figure 1(a) shows that Fh-CGH has the same high fidelity to recreate the input image as that of a Fr-CGH, even when $Nf \gg 1$. Meanwhile, Fh-CGH requires only about 2/3 computation time of Fr-CGH [Fig. 1(b)]. These results indicate the omission of the phase $\mathcal{P}$ in Eq. (1) will not affect the display performance but benefit the encoding process.

The quadratic phase $\mathcal{Q}$ in Eq. (2) is a key term in the Fh-CGH. Although the diffraction pattern of Fraunhofer is the same as that of FT, mathematical analysis reveals $\mathcal{Q}$ can cancel the quadratic phase related to the hologram coordinate in the reconstruction. It means Fh-CGH can be applied in a large DOF scene just as Fr-CGH. So Fh-CGH is different from Fourier CGH, in which the reconstructed images are near the focal plane and have a shallow DOF.

In fact, the computational process of Fh-CGH is equivalent to virtually placing lenses clingy to the front surface of planar objects. The focal length of each lens is equal to the distance between the object and the hologram. For complex 3D objects, this is troublesome (and nearly impossible) to be implemented in optical holography but convenient in the CGH. Since the virtual lenses are in the front of the objects in recording, real lenses are not needed for imaging in optical reconstruction.

To demonstrate the concept, we calculate two Chinese characters lying in the Fresnel region ($Nf \sim 410$ and 540). They are parallel to the hologram. Random phases are used to encode both Fr-CGH and Fh-CGH into Kinoforms. Optical reconstruction setup is shown in Fig. 2(a), where a 532 nm laser is expanded to illuminate a phase-only spatial light modulator (SLM; Holoeye Pluto, 1920 * 1080 with pixel pitch 8 μm). Real images are projected to a scattering screen in different distances and captured by camera. No Fourier lens is used. The performances of Fh-CGH [Figs. 2(c) and 2(e)] are consistent with Fr-CGH [Figs. 2(b) and 2(d)], especially for focusing and defocus effects. It indicates Fh-CGH can maintain as good of a performance as Fr-CGH, even for objects in the Fresnel region.

For off-axis slanted planar objects, we can also derive the field distribution on the hologram through rotation transformation and modified paraxial approximation [16]:

$$\mathcal{O}_H(x_H, y_H) = \{\exp[j2\pi(z_c + r_0)/\lambda]/j\lambda r_0\} \iint \mathcal{O}_o(x_l, y_l) \times \mathcal{S}(x_l, y_l) \exp[-j2\pi(x'_H x_l + y'_H y_l)/\lambda r_0] \mathrm{d}x_l \mathrm{d}y_l, \quad (3)$$

where $\mathcal{S} = \exp[j\pi(x_l^2 + y_l^2)/\lambda r_0]$, $x'_H = r'_{11}(x_H - x_c) + r'_{21}(y_H - y_c) - r'_{31}z_c - r'_{31}r_0$, and $y'_H = r'_{12}(x_H - x_c) + r'_{22}(y_H - y_c) - r'_{32}z_c - r'_{32}r_0$ with $r_0 = [(x_H - x_c)^2 + (y_H - y_c)^2 + z_c^2]^{1/2}$. Here, $(x_H, y_H, 0)$, $(x_l, y_l, 0)$ are the Cartesian coordinates of the hologram plane and the local object plane. r'_{ij} $(i, j = 1, 2, 3)$ are the elements of the rotation matrix related to the local and global Cartesian coordinate. (x_c, y_c, z_c) is the object's centroid in the global coordinate. r_0 is the distance between the object's centroid and the hologram pixel. Equations (1) and (3) can be found similar in form, and thus, the statements about Fh-CGH in the case of the parallel plane can be applied for the case of an off-axis slanted plane. The quadratic phase $\mathcal{S}$ can also be discarded and will not affect the display performance. Using a fast Fourier transform numerical algorithm, it is easy to calculate the FT for the parallel plane case but inconvenient for the slanted plane case because of the necessity of interpolations [10,13]. If a 3D object is regarded as a combination of triangle patches, the FT of $\mathcal{O}_o(x_l, y_l)$ can be analytically calculated to reduce the computational complexity [12,13,16]. The remaining problem is to apply a digital diffuser into the analytical algorithm to enlarge the viewing angle and make the object larger than the hologram.

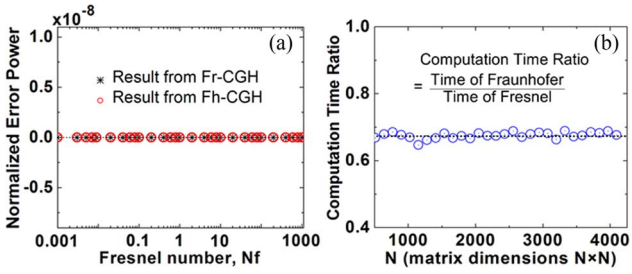

Fig. 1. (Color online) (a) Normalized error power between the intensities of holographic reconstructed image and original input object for different Fresnel numbers. (b) Comparison of computation time between Fh-CGH and Fr-CGH, while Nf = 1.

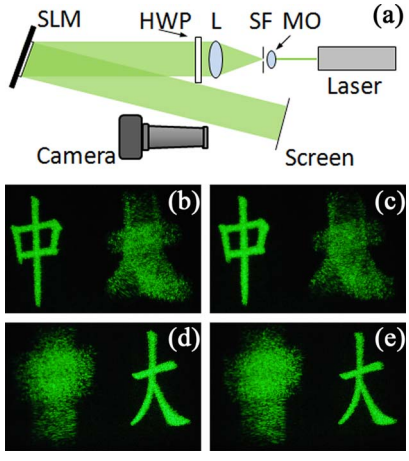

Fig. 2. (Color online) (a) Setup for optical reconstruction. MO, microscope objective; SF, spatial filter; L, lens; HWP, half-wave plates. Reconstruction in 800 mm ($Nf \sim 410$) for (b) Fr-CGH and (c) Fh-CGH and in 1100 mm ($Nf \sim 540$) for (d) Fr-CGH and (e) Fh-CGH.

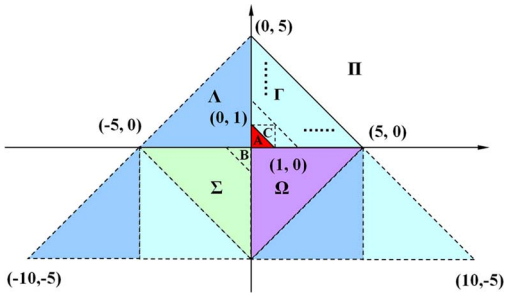

Fig. 3. (Color online) Scheme of the FT calculation of diffusive triangle using basic-triangle tiling method.

Here, we develop a basic-triangle tiling diffuser to solve the problem. Figure 3 shows the schematic diagram. The FT of the small basic triangle "A" with vertices as (0,0), (1,0), (0,1), denoted by $\mathcal{F}_A(u,v)$, can be deduced analytically [12,13]. With the help of the symmetry and the linear phase shifting operations, the FT of other basic triangles can be obtained through $\mathcal{F}_A$, e.g. $\mathcal{F}_B(u,v) = \mathcal{F}_A(-u,-v)$ and $\mathcal{F}_C(u,v) = \mathcal{F}_A(-u,-v)\exp[-j2\pi(u+v)]$. Hence, the FT of the middle triangle "Γ", $\mathcal{F}_\Gamma$, can be obtained from the superposition of the basic triangles. The FT of other middle triangles (e.g. Λ, Σ, Ω) can then be elicited through $\mathcal{F}_\Gamma$ with similar operations. Finally, the FT of the large fiducial triangle "Π" with vertices as $(-10,5)$, (10,5), (0,5), which contains hundreds of basic triangles, can be calculated analytically. If each basic triangle adds a random phase and they are different in between, it is equivalent to add a random diffuser to "Π." So the FT of the fiducial diffusive triangle can be achieved analytically. Using the affine transform, Fraunhofer diffraction field of an arbitrary slanted triangle can be obtained by

$$\mathcal{O}_H(x_H,y_H) = \frac{\exp[j2\pi(z_c+r_0)/\lambda]}{j\lambda r_0}(a_{22}a_{11}-a_{12}a_{21}) \times \exp\left(-j2\pi\frac{a_{13}x'_H+a_{23}y'_H}{\lambda r_0}\right) \times \mathcal{F}_\Pi\left(\frac{a_{11}x'_H+a_{21}y'_H}{\lambda r_0},\frac{a_{12}x'_H+a_{22}y'_H}{\lambda r_0}\right), \quad (4)$$

where $a_{11} = (x_l^2 - x_l^1)/20$, $a_{12} = (2x_l^3 - x_l^2 - x_l^1)/20$, $a_{13} = (2x_l^3 + x_l^2 + x_l^1)/4$, $a_{21} = (y_l^2 - y_l^1)/20$, $a_{22} = (2y_l^3 - y_l^2 - y_l^1)/20$, $a_{23} = (2y_l^3 + y_l^2 + y_l^1)/4$. $(x_l^i, y_l^i, 0)$, $i = 1, 2, 3$, are the vertices of the input triangle in the local coordinate. Because we have deduced the FT of a deterministic diffusive triangle, and it only requires affine transformation once, this approach maintains the efficiency of the analytical method that generates a hologram pixel by pixel. It need not use the discrete numerical algorithm, which may cause numerical errors when undersampling. Such pixel-independent calculation in a hologram is also very suitable for a graphics processing unit parallel computation.

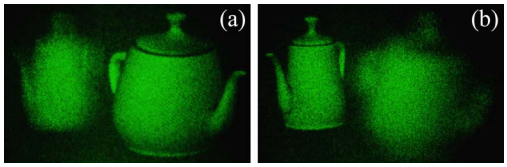

Fig. 4. (Color online) Optical reconstruction results of two 3D teapots. Reconstruction in (a) 800 mm and (b) 1100 mm.

Optical reconstruction is carried out to verify the validity of the analytical Fh-CGH for an arbitrary 3D object. The 3D scene (40 mm × 22 mm × 314 mm, which is larger than the SLM) contains two 3D teapots. Mouths of the teapots are respectively located at the distances of 800 and 1100 mm from the hologram to ensure that they are in the Fresnel region. The optical setup is the same as Fig. 2(a). High- quality reconstruction results are shown in Fig. 4. The basic-triangle tiling diffuser of the 3D object supplies a continuous and smooth surface, which performs a good solid effect. The shading in teapots adds a vivid feeling of curvature. When the front fat teapot is focused [Fig. 4(a)], it becomes clear and the rear slim teapot turns to vague, and vice versa [Fig. 4(b)]. This defocus effect gives an impressive depth sensation and a strong 3D feeling.

In conclusion, we demonstrated that the Fh-CGH can be employed in 3D imaging from the Fresnel to the far-field region for accelerating computation. We developed an analytical Fraunhofer-based algorithm to compute the diffusive 3D scene and obtained high-quality reconstructions. We believe for 3D display purposes, Fh-CGH may potentially benefit various CGH methods using Fresnel encoding, even the incoherent multiple-viewpoint-projection method [17].

This work is supported by the National Natural Science Foundation of China (NSFC) (10804131, 10874250, 11074311), the Fundamental Research Funds for the Central Universities (FRFCU) (20093000031 61450), and the Guangdong National Science Foundation (GDNSF) (10451027501005073).

References

1. J. W. Goodman, *Introduction to Fourier Optics* (Roberts & Company, 2004).
2. T. C. Poon, ed., *Digital Holography and Three-Dimensional Display* (Springer, 2006).
3. S. A. Benton and V. M. Bove, Jr., *Holographic Imaging* (Wiley, 2008).
4. P. A. Blanche, A. Bablumian, R. Voorakaranam, C. Christenson, W. Lin, T. Gu, D. Flores, P. Wang, W. Y. Hsieh, M. Kathaperumal, B. Rachwal, O. Siddiqui, J. Thomas, R. A. Norwooe, M. Yamamoto, and N. Peyghambarian, Nature **468**, 80 (2010).
5. W. X. Zhao, Q. H. Wang, A. H. Wang, and D. H. Li, Opt. Lett. **35**, 4127 (2010).
6. Y. Y. Pu, J. W. Dong, B. C. Chen, Y. Z. Liu, and H. Z. Wang, Opt. Lett. **35**, 3279 (2010).
7. T. Shimobaba, T. Ito, N. Masuda, Y. Ichihashi, and N. Takada, Opt. Express **18**, 9955 (2010).
8. H. Sakata and Y. Sakamoto, Appl. Opt. **48**, H212 (2009).
9. M. Bayraktar and M. Ozcan, Appl. Opt. **49**, 4647 (2010).
10. K. Matsushima, H. Schimmel, and F. Wyrowski, J. Opt. Soc. Am. A **20**, 1755 (2003).
11. L. Yu and M. K. Kim, Opt. Express **13**, 5621 (2005).
12. H. Kim, J. Hahn, and B. Lee, Appl. Opt. **47**, D117 (2008).
13. L. Ahrenberg, P. Benzie, M. Magnor, and J. Watson, Appl. Opt. **47**, 1567 (2008).
14. J. P. Waters, J. Opt. Soc. Am. **58**, 1284 (1968).
15. J. T. Kiwaki, T. Shimobaba, N. Masuda, and T. Ito, Opt. Lett. **35**, 1112 (2010).
16. Y. Z. Liu, J. W. Dong, Y. Y. Pu, B. C. Chen, H. X. He, and H. Z. Wang, Opt. Express **18**, 3345 (2010).
17. N. T. Shaked, B. Katz, and J. Rosen, Appl. Opt. **48**, H120 (2009).